Wettability of Electroless Ni in the Under Bump Metallurgy with Lead Free Solder

BI-LIAN YOUNG,[1] JENQ-GONG DUH,[1] and BI-SHIOU CHIOU[2]

1.—National Tsing Hua University, Department of Materials Science and Engineering, Hsinchu, Taiwan. 2.—National Chiao-Tung University, Department of Electronics Engineering, Hsinchu, Taiwan

This study investigates the wettability of several lead-free solders, including Sn, Sn-Ag, and Sn-Bi, on electroless Ni (EN) with various phosphorus contents. The role of phosphorus on solder wettability is studied. Microstructure evolution in the lead-free solder/EN joint is investigated with the aid of electron probe microanalyzer (EPMA) to relate metallurgical reactions between the solder and the EN. The Sn solder exhibits better wettability on EN, while the Sn-Bi solder has a larger contact angle. Wettability degrades as the phosphorus content in EN decreases. The dependence of wetting angle on the phosphorous content can be attributed to the surface roughness and density of EN, along with the interfacial reaction between the solders and EN. An EPMA analysis reveals the presence of a Sn-Bi-Ni-P solid solution at the interface of solder/EN joints due to the interdiffusion of major constituent Ni and Sn. The interaction zone of the solid solution increases with increasing temperature. Wettability of Pb-free solders on EN degrades with the presence of NiO due to oxidation or the existence of Ni_3P due to precipitation after annealing. For an adequate wetting behavior in the Sn (Sn-Bi, Sn-Ag)/EN joint, EN deposited with phosphorus contents in the range of 9 to 12 wt.% is suggested.

Key words: Lead-free solder, electroless nickel, wettability, interfacial microstructure

INTRODUCTION

Flip-chip technology offers the greatest 1/0 number and packaging density among the currently available chip bonding technologies. It is anticipated that the flip chip technology including both flip chip in package (FCIP) and flip chip on board (FCOB) will grow very rapidly in the coming years.[1,2] The preliminary steps for flip chip technology is the manufacturing of bumps on the die. An under bump metallization (UBM) is a multi-layer combination whose functions include adhesion to the terminal electrode, a diffusion barrier between the solder and terminal electrode, and wetting for soldering. Available UBM structures are Cr/CrCu/Cu, Ti/Cu/Cu, Ti-W/Cu/Cu,[3] or electroless nickel (EN)/Cu.[3–5] The EN process does not require a costly vacuum process, nor electrical power supply, and is a low cost bumping process. The Cu-based UBM has been found to be incompatible with eutectic Sn-Pb solder due to the rapid reaction of the Sn with Cu and the spalling of Cu-Sn intermetallic compounds.[6] On the other hand, a Ni-based UBM is of interest in low cost flip chip technology due to a slower chemical reactions with Sn-rich solders compared to Cu-based UBMs. In addition, the EN exhibits lower residual intrinsic stress compared with Ni films prepared by vacuum deposition.[6] The characteristics of the electroless nickel deposit, such as adequate solderability, corrosion resistance, uniform thickness, and selective deposition, make the electroless nickel deposit a diffusion barrier.[7]

The applications of EN for interconnection with solders rely on the solderability and the interactions between nickel and solder. The factors such as phosphorous content of the EN, soldering temperature, composition of the solder alloys, and flux influence solderability of the EN.[7,8] Recently, Ni bumps have been investigated for potential applications. Feldstein and Thomann studied the solderability of EN by using quantitative contact angle measurements. Ni-P de-

(Received August 14, 2000; accepted February 16, 2001)

Table I. Bath Composition and Operating Conditions of Electroless Ni-P Plating

Nickel sulfate $NiSO_4 \cdot 6H_2O$	40 g/l
Sodium succinate $Na_2C_4H_4O \cdot 6H_2O$	32 g/l
Sodium hypophosphite $NaH_2PO_2 \cdot H_2O$	27 g/l
Stirring rate	100 rpm
pH	4.0~6/7
Load	10 (cm^3/cm^2)

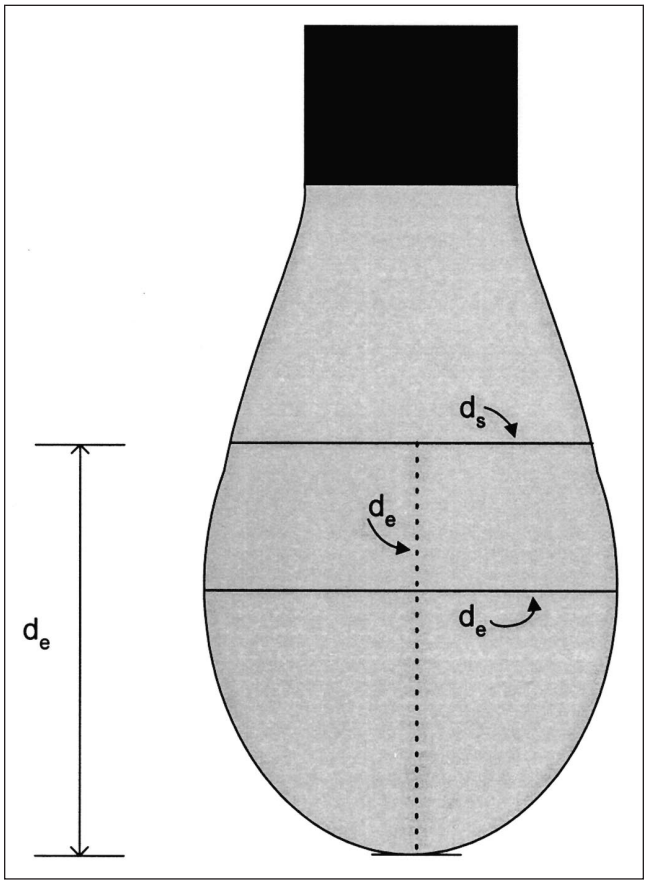

Fig. 1. Pendent drops profile.

posits of low phosphorous contents (<6%) exhibited the best solderability characteristics. Hajdu also found that deposits with medium phosphorous contents, 5–8 wt.%P, were more solderable than those with higher phosphorous contents, ~11 wt.%P. Aoki reported that EN deposits with 7 wt.% phosphorus exhibited superior solderability.[7] Fang et al. found that the solderability of EN deposits decreased when both phosphorus content and temperatures decreased.[8]

In the pursuit of green product in today's industry, the harmful effect of lead on the environment and human health, coupled with the proposed legislation, have prompted the search for lead-free solders for electronic packaging application.[9,10] Two groups of Pb-free solders are proposed: Sn-rich solders, such as Sn-Ag, or Sn-Sb alloys, for high temperature soldering, and Sn-Bi or Sn-In eutectic alloys for low temperature soldering. One key technical issue recognized with Sn-base solders is the need to develop a good diffusion barrier metallurgy to prevent excessive dissolution of copper base metal during soldering and to improve solderability as well as solder joint reliability. However, few studies concerning the solderability of lead-free solders on Ni-P surface has been reported. The purpose of this study is first to investigate the microstructure evolution in Pb-free solder/EN joints. The lead-free solders include pure Sn, eutectic Sn-3.5 wt.% Ag, and Sn-58 wt.% Bi. The effects of phosphorous contents in the EN on the wettability are probed. In addition, the influence of the soldering temperature and the surface condition of EN after thermal treatment on the wetting behavior will be investigated.

Table II. Compositions of As-Fabricated Ni-P Substrates

pH	Ni (wt.%)	P (wt.%)
4.0	86.69 ± 0.61	13.30 ± 0.61
5.2	87.47 ± 0.77	12.52 ± 0.77
6.0	91.47 ± 0.18	8.52 ± 0.18
6.7	93.72 ± 0.46	6.28 ± 0.46

EXPERIMENTAL

Eutectic solder alloys were fabricated from raw materials including pure tin, pure bismuth, and silver (purity >99.9%). Raw materials with appropriate weight were cleaned and put into a quartz tube evacuated to 10^{-2} atm. The tube was placed in a furnace at 1050°C for 8 h and continuously shaken during melting for the purpose of homogenization. Finally, the tube was taken out and quenched in cold water. The solder alloys were obtained after the tube was broken. The compositions of as-fabricated solder alloys were evaluated with an electron probe microanalyzer. The measured compositions were 96.5 wt.%Sn-3.4 wt.% Ag and 44.4wt.%Sn55.6wt.%Bi, respectively. The as-fabricated Sn-Ag alloy is nearly identical to the eutectic 96.5Sn-3.5Ag in the Sn-Ag phase diagram.[11] However, the composition of as-fabricated Sn-Bi alloy is a little deviated from the eutectic 42Sn-58Bi, possibly due to Bi loss in the melting.

The ceramic used in this study was a commercial α-96%Al_2O_3 substrate. The Al_2O_3 substrate was cleaned ultrasonically in alcohol and then acetone, for 10 min. Table I gives the chemicals and parameters in the electroless plating solution used in this study. The working temperature of plating was maintained at 85°C ± 0.5°C where the solution remained stable and the deposition rate was high. The pH value of the plating solution ranging from 4.0 to 6.7 was controlled with a 50 vol.% H_2SO_4 solution.

The microstructures of solder alloys, including pure Sn, eutectic Sn-Ag, and Sn-Bi on Ni-P/Al_2O_3 substrates were analyzed with a scanning electron microscope. The compositions of intermetallic compounds

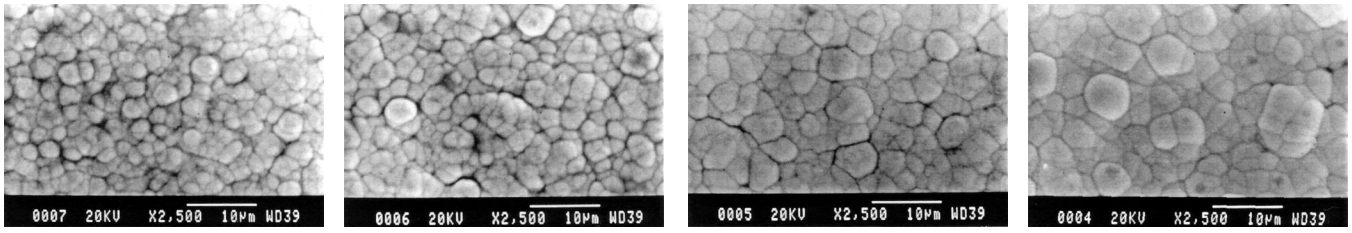

Fig. 2. Surface morphologies of EN deposited on Al_2O_3 substrate with various pH values, (a) pH = 3.9, (b) pH = 4.0, (c) pH = 5.2, and (d) pH = 6.0.

and elemental distribution of solder/multi-metallization joints were quantitatively measured by an electron-probe microanalyzer (EPMA) along a trace line across the interfacial boundary in the joint assembly.

An x-ray diffractometer with a wavelength of Cu Ka (γ = 1.5406 Å) was used to examine the phase and crystal structure of precipitate Ni_3P upon the heat treatment of EN. The x-ray was generated by an anode operated 30 kV and 20 mA, and the scanning rate was 4°/min. In addition, Auger and electron spectroscopy for chemical analysis (ESCA) were used to detect the composition of EN after heat-treatment.

The as-metallized EN/Al_2O_3 substrates were cut into disks of 0.9 × 4.4 cm. Some of the EN/Al_2O_3 samples were annealed at 350°C for 1 to 3 hours in a low-temperature drying oven to produce the nickel oxide and precipitated phases (Ni_3P) of EN. Finally, the EN/Al_2O_3 substrates with different phosphorous contents and Ni_3P precipitation were cleaned ultrasonically in deionized (DI) water.

A contact angle analyzer system was used to measure interfacial phenomena such as surface tension, surface energy, and contact angle. The solder alloys/EN/Al_2O_3 joint with rosin mildly activated (RMA) flux were placed in the environment chamber. A temperature controller manipulated the temperature of the environment chamber. After the temperature of an environment chamber was at the desired setting, the alloys inside the needle melted. A syringe plunger was pushed to form a pendant drop or a sessile drop on a substrate. The solderNi-P/Al_2O_3 system was mingled with RMA flux and then melted at 1.2 T_m, (T_m means the melting temperature of the specific solder) soldering for 30 sec. The solder joints were formed after air-cooling. The solder alloys/EN/Al_2O_3 joints without RMA flux were used to study the effect between wettability and nickel oxide of EN. Once the drop was formed, live images were continuously captured of the contact angle.

The surface tension is calculated as follows:

$$\gamma = \rho_L \cdot g \cdot d_e^2/H \quad (1)$$

where ρ_L is the liquid density, g is the gravitation constant, d_e is the maximum drop diameter, and H is the dimensionless quantity. The pendent drop profile is shown in Fig. 1.

RESULTS AND DISCUSSION

The phosphorus content of as-deposited Ni-P/Al_2O_3 substrates analyzed by EPMA are listed in Table II. The

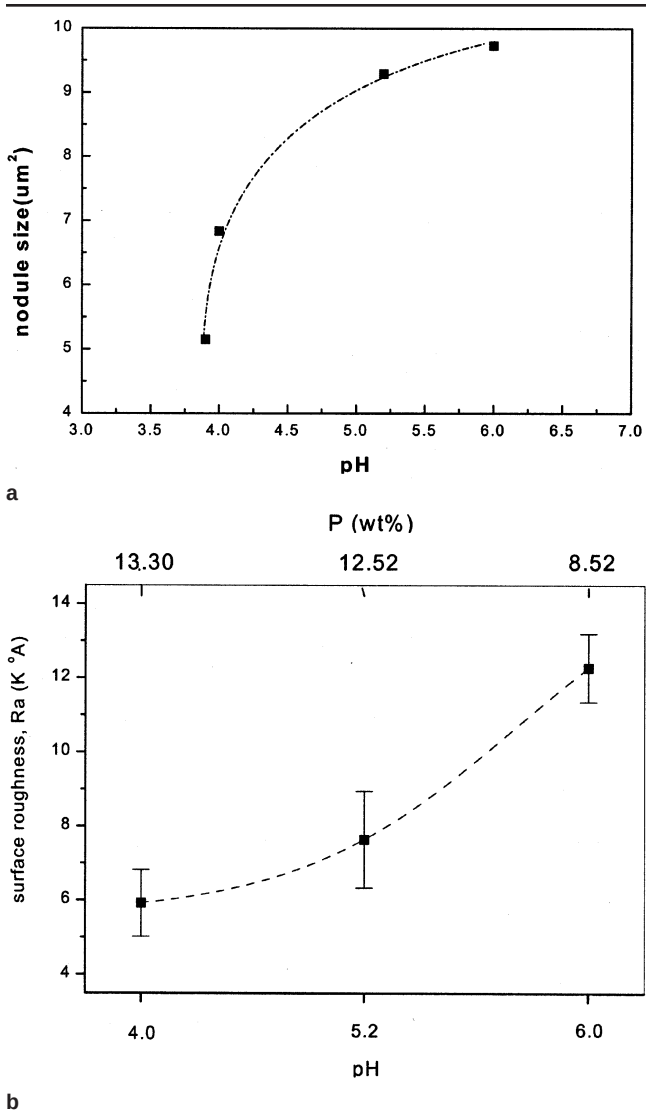

Fig. 3. (a) Nodule size and (b) surface roughness of EN as a function of pH value during deposition.

phosphorus content obtained at various pH values of 6.7, 6.0, 5.2, 4.0, are 6.0 wt.%, 7.3 wt.%, 9.2 wt.%, and 12 wt.%, respectively. Figure 2 shows the surface morphology of various as-deposited EN on Al_2O_3 substrates. The nodule size of the EN films increases as the pH value increases. The nodule size and surface roughness as a function of pH value are shown in Fig. 3a and b, respectively. The surface roughness of as-deposited EN increases with the pH values.

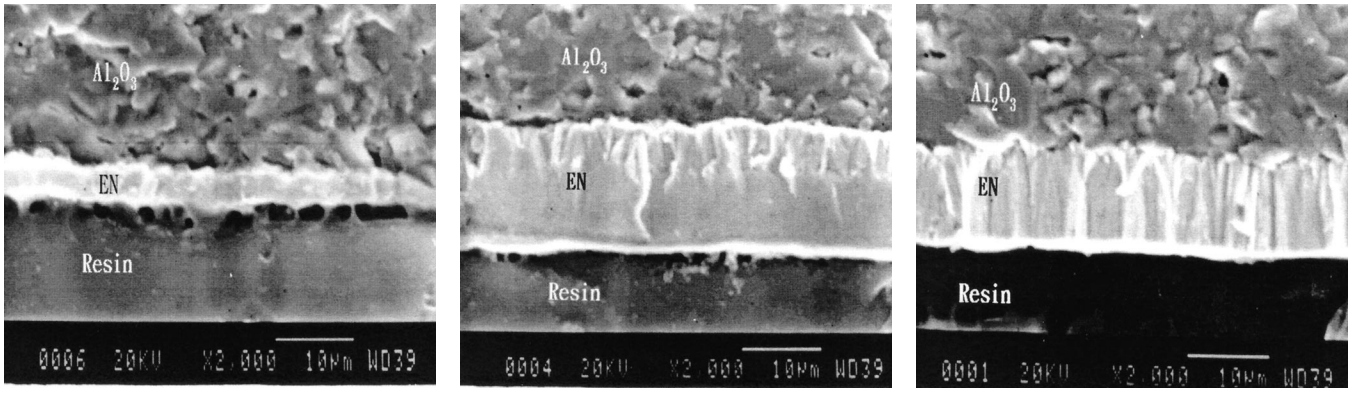

a b c

Fig. 4. Cross sectional views of EN deposited on alumina with various pH values of bath solution, (a) pH = 4.0, (b) pH = 5.2, and (c) pH = 6.0.

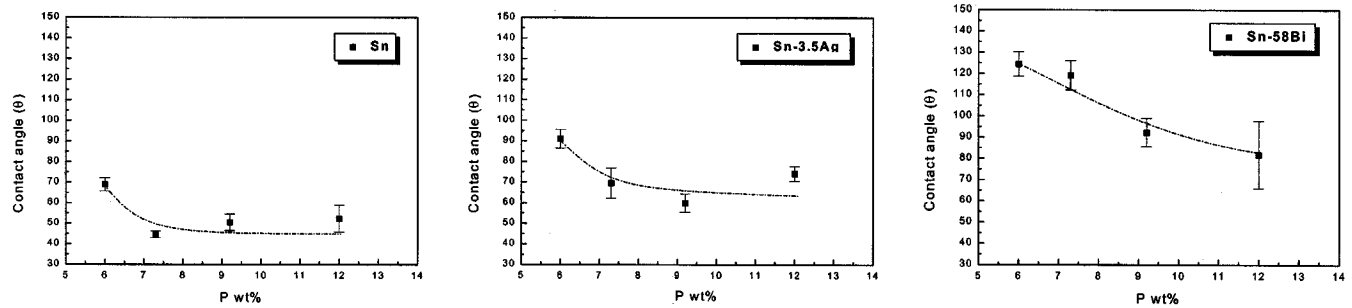

a b c

Fig. 5. The static angle of various lead free solder alloys on EN as a function of P wt.%, (a) pure Sn, (b) Sn-3.5Ag, and (c) 42Sn-58Bi.

Cross-sectional SEM images of the EN/Al_2O_3 are indicated in Fig. 4. EN deposited at high pH values of 6.0 exhibit a columnar microstructure, while that deposited at a lower pH value of 4.0 results in the amorphous features. The mixed mode of columnar and amorphous microstructure appears in EN plated at pH 5.2.

The contact angles of lead-free solders, including pure Sn, eutectic SnBi, and Sn-Ag, on the metallization are evaluated. The contact angles of lead-free solders on electroless nickel deposited with various pH values are shown in Fig. 5. The contact angles of pure Sn on EN with phosphorous contents from 6.0 to 12.0 wt.% are in a range between 45 and 70 degrees, while that of Sn-3.5Ag/EN and 42Sn-58Bi/EN are ranged from 60° to 90° and 80° to 125°, respectively.

Among the three lead-free solders, pure Sn exhibits the best wettability on electroless Ni. The Sn-Bi solder displays a relatively large contact angle. Nonwetting is observed in the Sn-Bi solder on EN with the phosphorous contents smaller than 9 wt.% as indicated in Fig. 5c.

Wettability of Sn, Sn-Ag, or Sn-Bi on the electroless Ni depends on the phosphorous content in EN. The lower the phosphorous content, the higher the contact angle. To achieve better wettability of the three lead-free solders on EN, a selection of EN with phosphorous contents larger than 9 wt.% are more appropriate. Lin et al.[12] reported that the contact angles of 63Sn-37Pb solders on EN generally decreased with lower pH values. A wetting balance measurement for the eutectic Sn-Bi solder showed contact angles of 57° and 76° on the Ni foil and Ni plate, respectively.[13] A similar study for the eutectic Sn-Ag solder on the Ni substrates were in the range of 76~83°.[14] The contact angle between eutectic Sn-Bi and EN is larger than that between eutectic Sn-Bi and pure Ni. The discrepancies become much larger if the P contents in EN are reduced. However, for the eutectic Sn-Ag, the wettability on EN (around 60~90°) is comparable to that of pure Ni (around 76~83°). In fact, a relatively better wettability with a contact angle less than 60° is observed for EN with P contents around 9 wt.%.

Table III. Measured Values of Surface Tension of Solder Alloys (Molten State)[15]

Alloy	42Sn-58Bi	Sn-3.5Ag	Sn
Surface tension, γ (dynes/cm)	319	431	530

The surface tension of solder and substrate plays an important role in determining wetting behavior. Table III lists the measured values of surface tension of Sn, Sn-Bi, and Sn-Ag alloys in the molten state.[15] Eutectic Sn-Bi has the lowest surface tension, while pure Sn has the largest surface tension. According to Young's equation:

$$\gamma_{sv} - \gamma_{si} = \gamma_{lv} \cos\theta_e \quad (2)$$

where θ_e is the equilibrium contact angle, γ_{sv} is the surface tension between solid and vapor, γ_{lv} is the

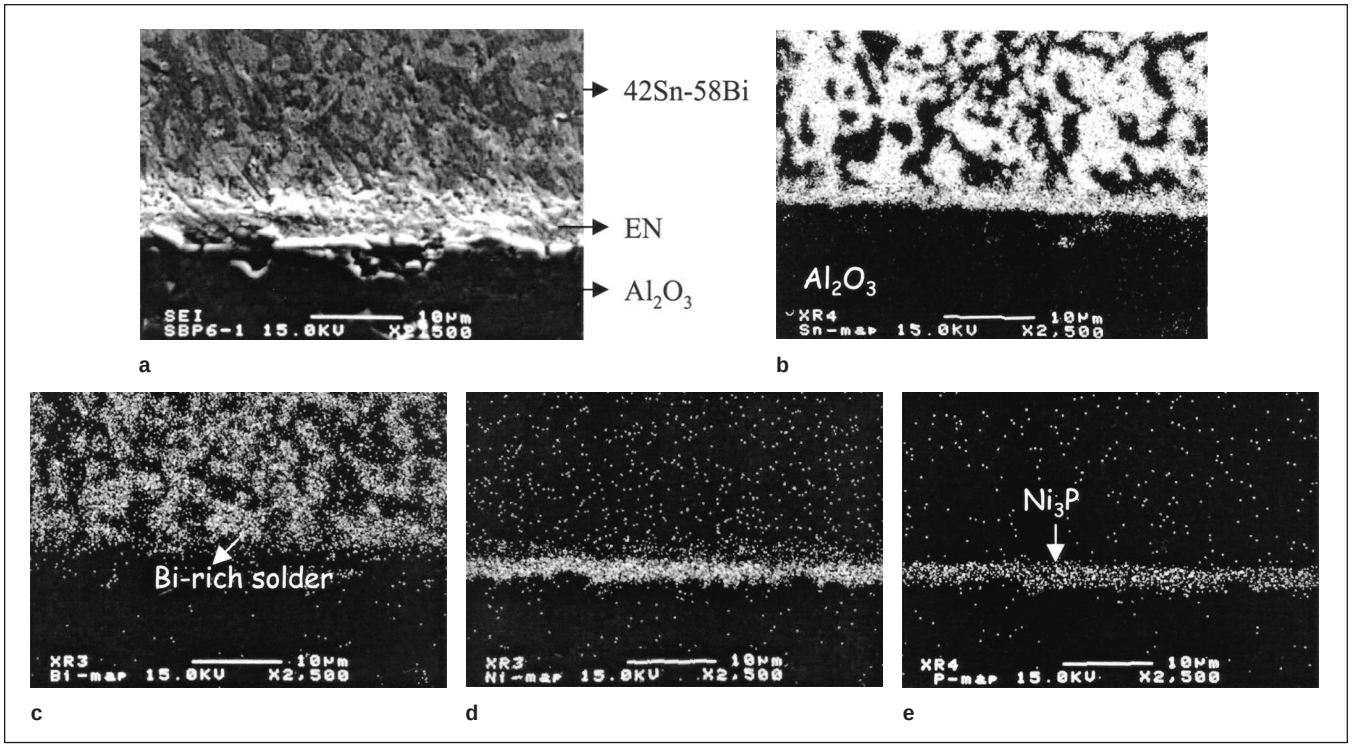

Fig. 6. Morphology of 42Sn-58Bi/Ni-6wt,%P joint reflowed at 165°C for 30 sec, (a) SEI image, (b) Sn x-ray mapping, (c) Bi x-ray mapping, (d) Ni x-ray mapping, and (e) P x-ray mapping.

surface tension between liquid and vapor, and γ_{sl} is the surface tension between liquid and solid. Wetting can be enhanced by larger values of γ_{sv} in combination with small values of γ_{lv} and γ_{sl}. Usually, the lower surface tension between liquid and vapor results in a smaller contact angle. However, the exact values of γ_{lv} and γ_{sv} are not known, so it is not feasible to evaluate the variation of contact angle among these three solders. It was proposed that the values of solid/vapor interfacial tension decreased as the phosphorous contents increased,[12] which would lead to a larger contact angle as the phosphorous contents are raised. However, this is not the case observed in this study. In fact, it was not possible to judge the wetting behavior by Young's equation. without a full knowledge of all the interfacial energies, including γ_{sv}, γ_{lv}, and γ_{sl}.

Nevertheless, the variation of contact angle with phosphorous content shown in Fig. 5 can be related to surface roughness. Figure 3b shows that the surface roughness of the as-deposited EN increases with pH. The surface roughness is reduced as the phosphorous content increases in the EN. The reduced roughness of the EN surface causes the solder to spread out more freely during reflow and thus the contact angle is decreased, as shown in Fig. 5.

As to the correlation between the surface roughness and spreading, an early model was carried out by Wenzel[19] to discuss the effect of surface roughness on wetting from a thermodynamic approach which predicts that the apparent contact angle decreases with the roughness ratio if the contact angle is less than 90°. A different prediction by Shuttleworth and Bailey,[20] however, pointed out that rough surfaces cause the contact angle to distort locally , and the contact angle increases with the surface roughness. This discrepancy between Wenzel and Shuttleworth was resolved by regarding the asperities as a series of energy barriers that must be overcome as the liquid front spreads over the surface.[21–23] Zhou and De Hosson[24] argued that rough grooves can be categorized into two types, i.e., radial and circular grooves in the middle of which a liquid drop is placed. Any type of grooves on a practical rough surface is a combination of these two types of grooves. The effect of substrate surface roughness on the wettability of eutectic Sn-Bi solders was recently investigated on Cu/Al_2O_3 substrates at 190°C.[25] The surface energy and thus the wetting mechanism of the solder are dependent on the surface roughness of the substrate, which in turn reflects variation in both the static and dynamic contact angles. During dynamic wetting, the wetting velocity of the solder drop decreases on the rough surface. However, the time to reach the static contact angle appears similar despite substrate surface roughness. As the solder drops reach a static state, the static contact angle increases with the substrate surface roughness. It is demonstrated that the wettability of solders degrades as the substrates become rough.

Soldering reactions are accompanied by the formation of intermetallic compounds or reaction products. The formation energy of the reaction product is larger than the capillary force. This suggests that the driving force of the wetting process is not only the surface energy balance as shown in the Young's equation, but also the free energy change during reaction. There

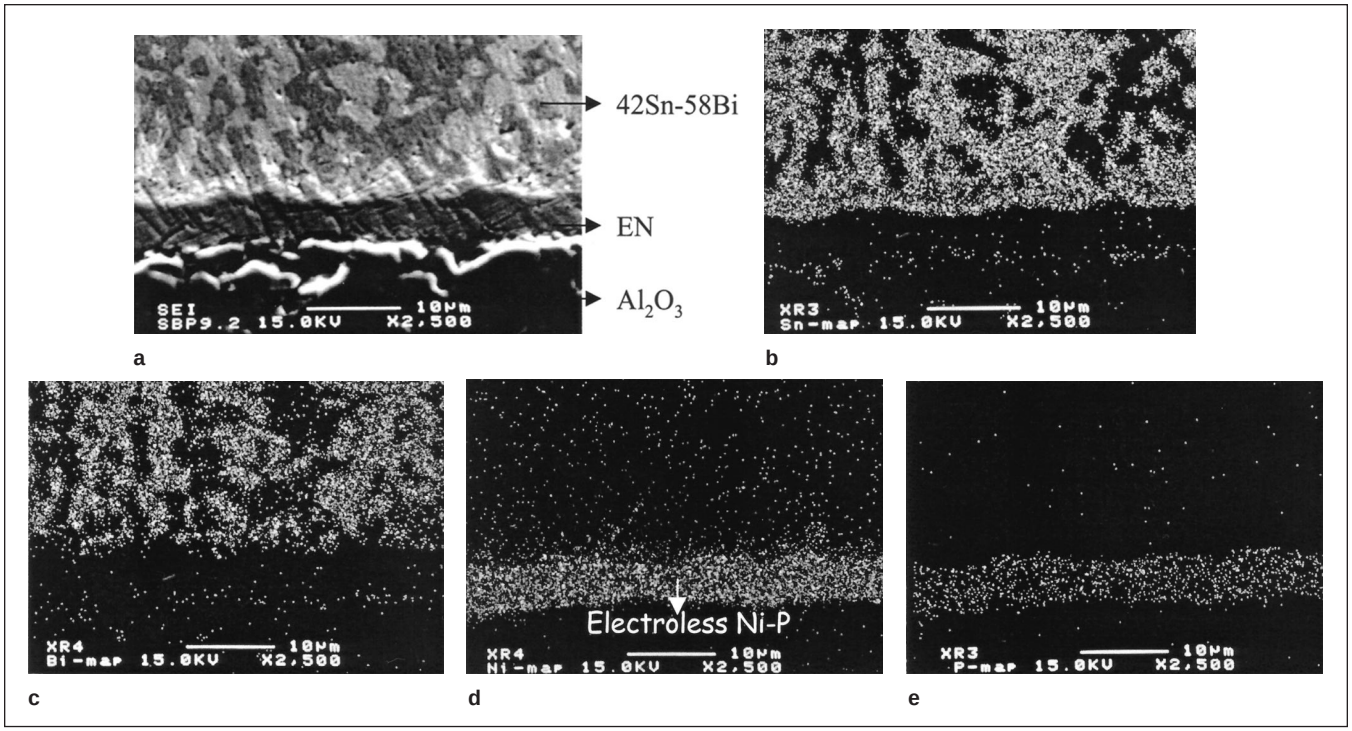

Fig. 7. Morphology of 42Sn-58Bi/Ni-9.2wt.%P joint reflowed at 165°C for 30 sec, (a) SEI image, (b) Sn x-ray mapping, (c) Bi x-ray mapping, (d) Ni x-ray mapping, and (e) P x-ray mapping.

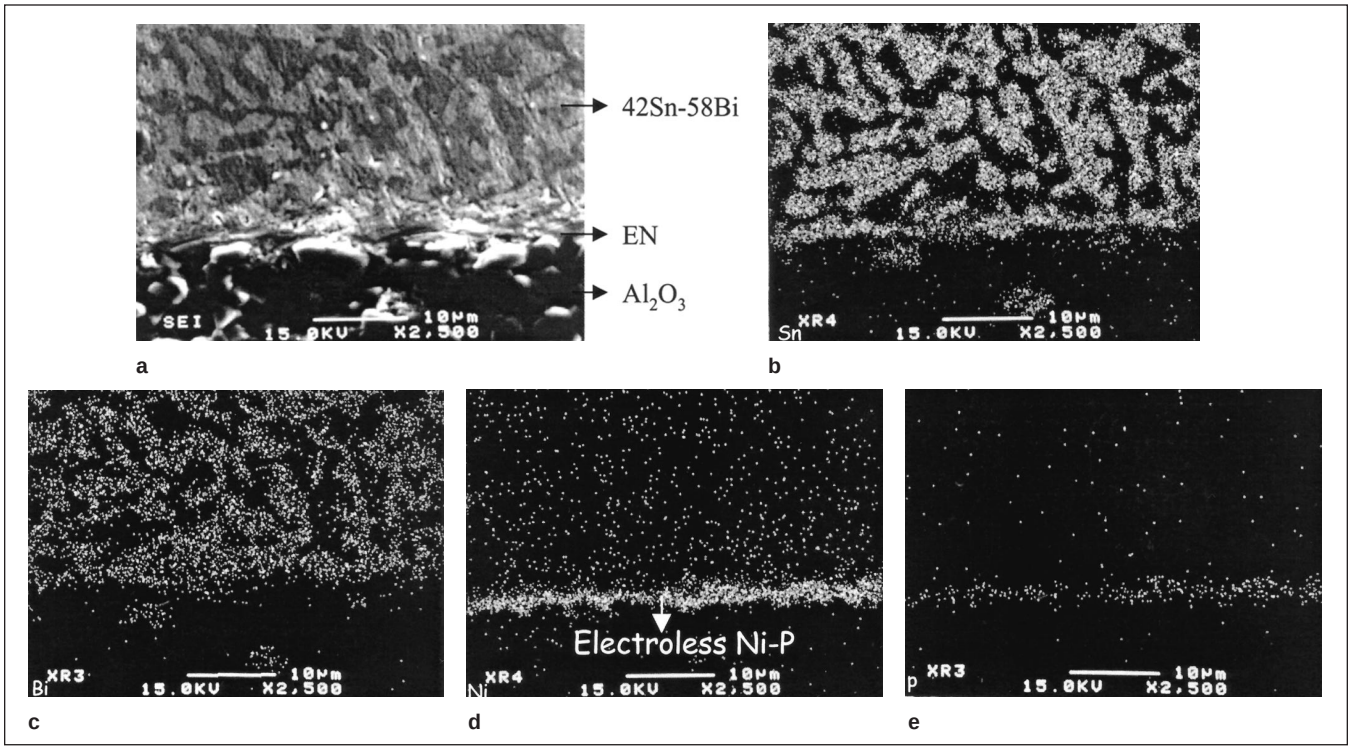

Fig. 8. Morphology of 42Sn-58Bi/Ni-12wt.%P joint reflowed at 165°C for 30 sec, (a) SEI image, (b) Sn x-ray mapping, (c) Bi x-ray mapping, (d) Ni x-ray mapping, and (e) P x-ray mapping.

exists interfacial reactions between solders and metallized substrates during soldering. Thus, a detailed investigation on the metallurgical interaction between solders and metallized substrate is required.

Figures 6–8 show the morphologies and x-ray mapping of 42Sn-58Bi solder reflowed at 165°C for 30 sec on electroless nickel with different phosphorous content. The lighter area in the solder bulk in Figs. 6b~8b indicates the Sn-rich region, the gray area is Bi-rich. From these micrographs, interfacial products between

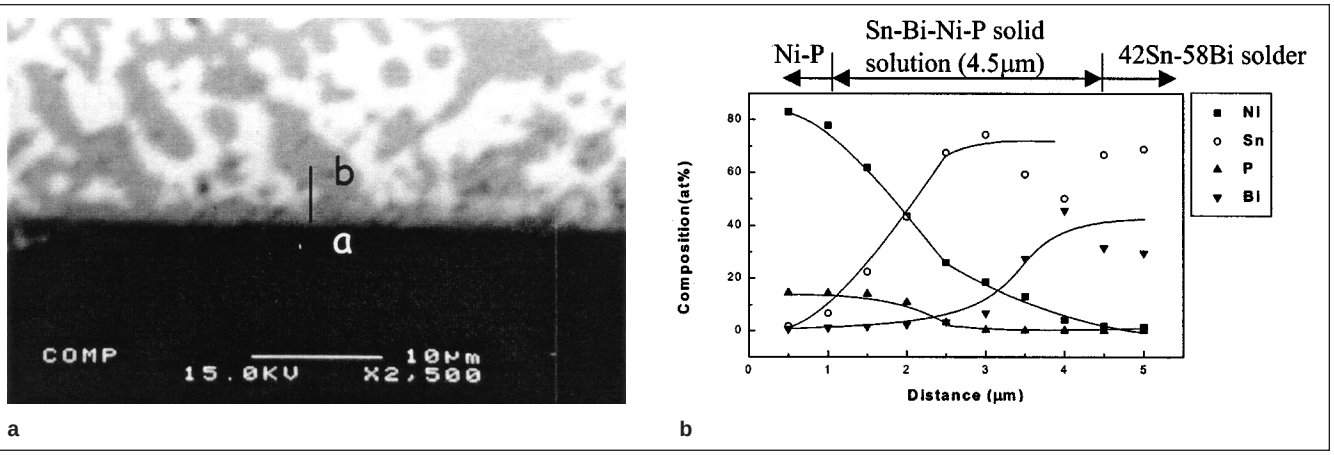

Fig. 9. Electron microprobe trace across the interface of the 42Sn-58Bi/Ni6wt.%Pjoint reflowed at 165°C for 30 sec , (a) cross section view, and (b) concentration profile corresponding to (a) along the trace line ab.

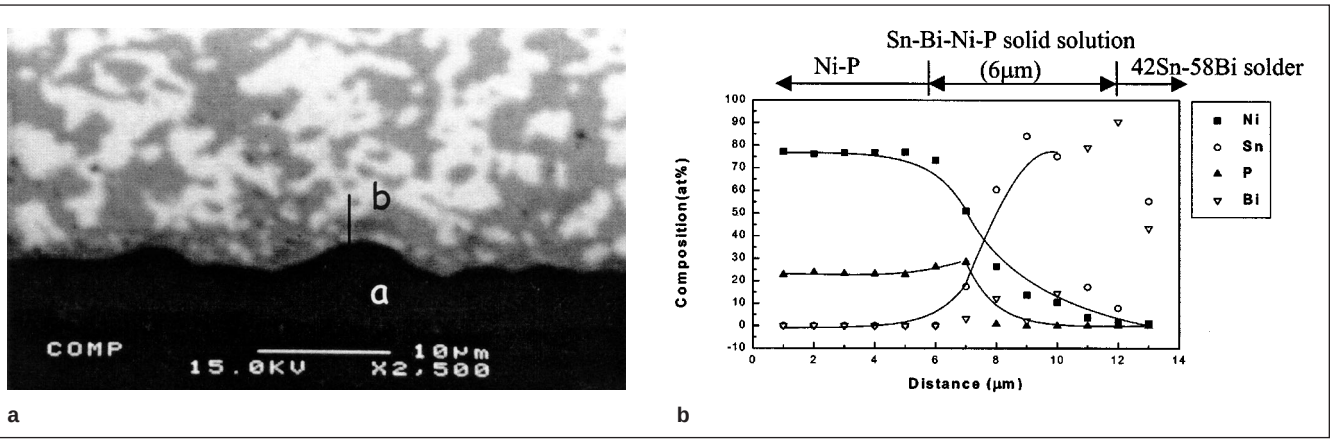

Fig. 10. Electron microprobe trace across the interface of the 42Sn-58Bi/Ni9.2wt.%P joint reflowed at 165°C for 30 sec, (a) cross section view, and (b) concentration profile corresponding to (a) along the trace line ab.

the EN and the solder bulk exist. EPMA quantitative analysis along the trace line across the interfacial region was conducted and concentration profiles for each constituent element were evaluated. Figures 9 and 10 represent the magnified cross sectional view of the interfacial region along with the corresponding concentration profile for the joint assembly Sn-Bi/EN (6.0 wt.%) and Sn-Bi/EN (9.2 wt.%), respectively. The reaction product was identified as a Sn-Bi-Ni-P solid solution, rather than the intermetallic compound. The interaction zone for the Sn-Bi solder on EN with 6.0 wt.% P is around 4.5 μm, as indicated in Fig. 9b, while it is increased to 6 μm for the Sn-Bi solder on EN with 9.2 wt.%P. This provides additional evidence that EN with a higher phosphorous content has better wettability for Sn-Bi solders, as shown in Fig. 5.

In Figs. 9b and 10b, Ni diffuses from the EN side toward the Sn-Bi bulk, while Sn moves from the solder side toward the EN layer. Thus a solid solution region of Sn-Bi-Ni-P forms. Enrichment of P near the interface between the EN layer and the solid solution occurs.

The degree of interfacial reaction with respect to the variation of phosphorous contents in EN can also be appreciated with the density change of EN. The densities of EN decreases with increasing phosphorous contents.[16] The lower density provides more channels for the elements Ni and Sn to diffuse toward each other. Consequently, EN with higher phosphorous contents exhibits a better wetting behavior in the Sn-Bi/EN joint, as revealed in this study.

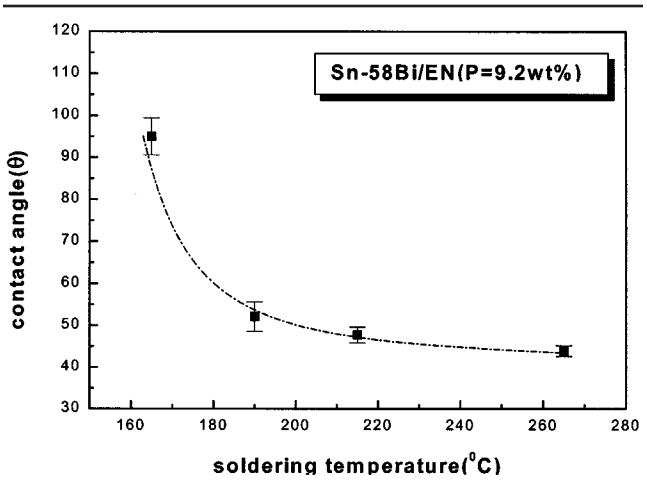

Fig. 11. The static angle of eutectic Sn-Bi soldered on Ni-9.2wt.% P at different soldering temperature.

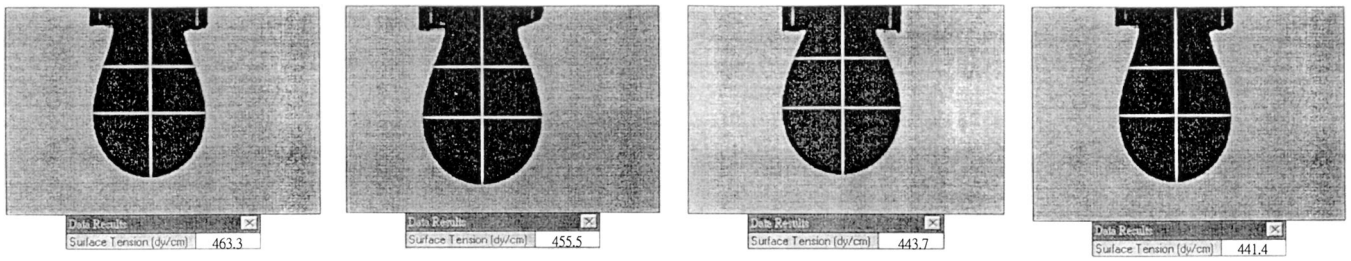

Fig. 12. Pendant drop images and surface tension of eutectic Sn-Bi solder at various temperature (a) 165°C, (b) 190°C, (c) 215°C, and (d) 240°C.

Table IV. The Surface Tension of 42Sn-58Bi Solder at Different Soldering Temperatures

Soldeirng temp. (°C)	165	190	215	240
Surface tension (dyne/cm)	463.3	455.5	443.7	441.4

THE EFFECT OF SOLDERING TEMPERATURE FOR EUTECTIC Sn-Bi SOLDER ON CONTACT ANGLE WITH EN (9.2 wt.% P)

EN with 9.2 wt.% P exhibits the best wettability for the Sn-Bi/EN joint. This joint assembly was used to study the effect of soldering temperature on the contact angle. Figure 11 shows the variation of contact angle for eutectic Sn-Bi solder on EN with 9.2 wt.% P as a function of soldering temperature. The contact angle reduces as the soldering temperature increases, and approaches a steady state around 40° at 265°C. The pendant drop images of the solder corresponding to various temperatures are shown in Fig. 12, with the evaluated surface tension listed in Table IV. The surface tension of Sn-Bi solder decreases slightly as the temperature increases.

In general, surface tension, the major parameter that determines the contact angle, is mildly temperature sensitive. However, viscosity is much more sensitive to temperature. According to the hydrodynamic theory of wetting, the excess capillary force is compensated by the friction term, assumed to be dominated by viscous dissipation in the wedge. It can be shown that the viscosity (η) is related to the volume, boiling point of the solder, and the operation temperature:[17]

$$\eta \cong \frac{Nh}{V} e^{\frac{3.8Tb}{T}} \qquad (3)$$

where N is Avogadro's number, h is the Planck constant, V is the volume of a mole of liquid, and Tb is the boiling point. Usually viscosity increases with lower temperature, slows down the drop of solder spreading, and reveals the larger contact angle. Increases in temperature decrease the viscosity and a smaller contact angle is achieved, as indicated in Fig. 11.

Cross sectional views of 42Sn-58Bi/Ni-9.2 wt.%P/Al_2O_3 joints soldered at temperature 165°C, 190°C, 215°C, and 240°C, for 30 sec are shown in Fig. 13a–d, respectively. Concentration profiles for each constituent element along a trace line across the solder/EN interface were evaluated by EPMA. A reaction zone exists between the solder bulk and EN layer after soldering. EPMA quantitative analysis reveals that this reaction zone is a solid solution of Ni-Sn-Bi-P, rather than an intermetallic compound. The concentration profiles for Bi, Sn, P, and Ni in the Sn-Bi/EN joint soldered for 30 sec at 165°C, 190°C, 215°C, and 240°C are shown in Fig. 14a–d. Ni and P diffuse from the EN layer toward the Sn-Bi solder bulk, while Sn and Bi move from the solder bulk toward the EN layer. The penetration depth for Ni into the Ni-Sn-Bi-P solid solution is increased from 2 μm to 4 μm when the soldering temperature is raised from 165°C to 240°C, as indicated in Fig. 14a and d. The deeper penetration of Ni is attributed to the elevated temperature during soldering. The interaction of Sn and Ni are accelerated with the soldering temperature, additional evidence for the reduced contact angle in the Sn-Bi/EN joint with increasing soldering temperature, as shown in Fig. 11.

THE EFFECT OF THE NiO AND Ni_3P PRECIPITATE FOR THE ELECTROLESS NICKEL AFTER ANNEALING UPON CONTACT ANGLE

The as-deposited EN is usually annealed to modify

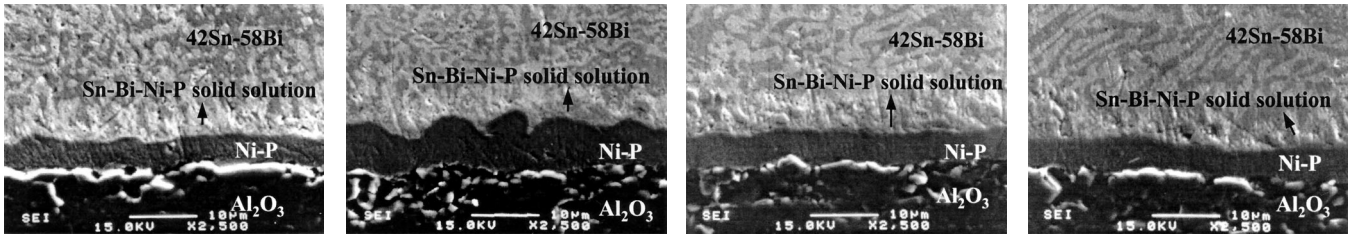

Fig. 13. Cross sectional views of the Sn-Bi/EN (9.2wt.% P) joint at different soldering temperatures (a) 165°C, (b) 190°C, (c) 215°C, and (d) 240°C.

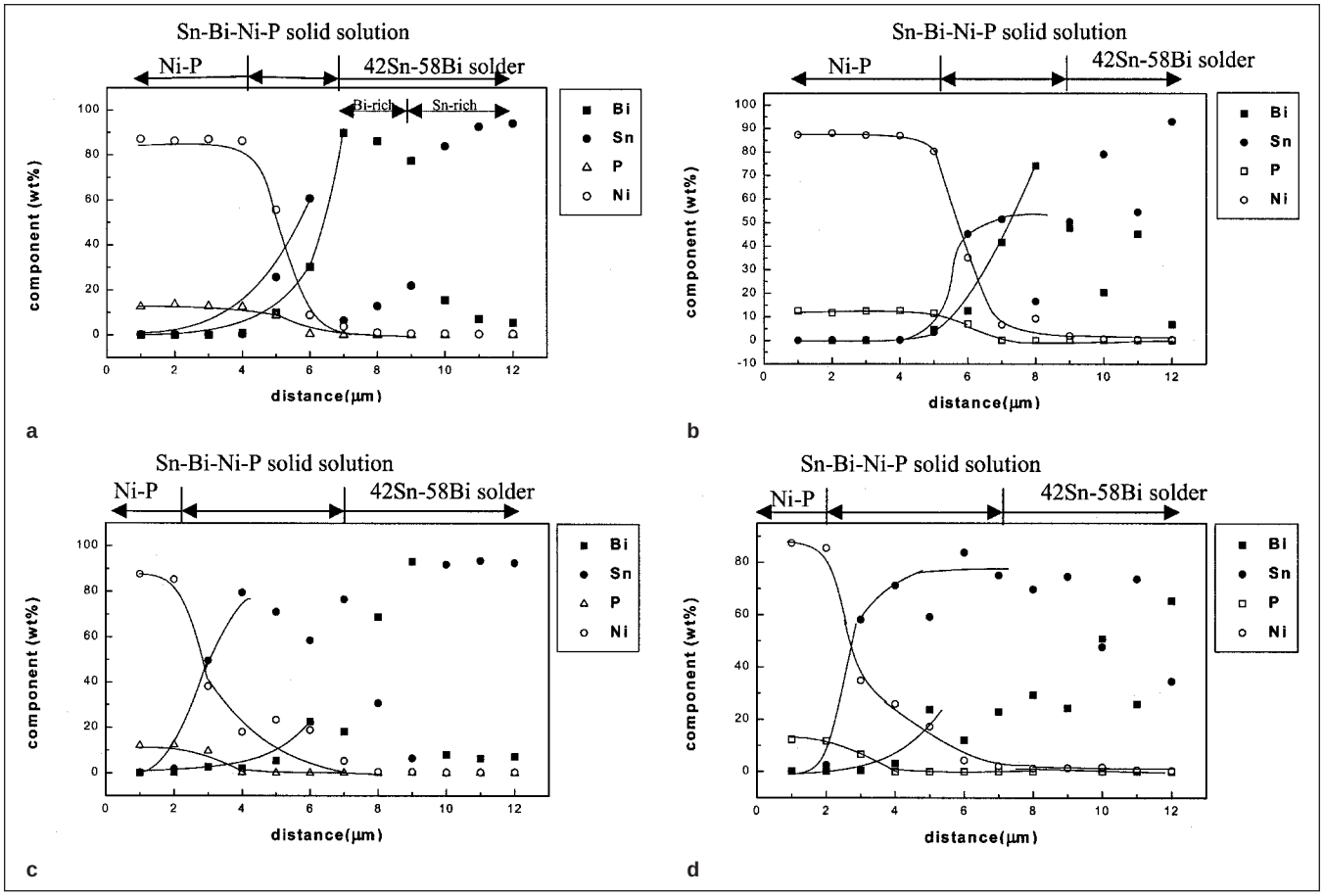

Fig. 14. Electron microprobe trace across the interface of the 42Sn-58Bi/Ni9.2wt.%P assembly soldered at (a) 165°C, (b) 190°C, (c) 215°C, and (d) 240°C.

the microstructure and phase to obtain the expected physical and chemical properties. To investigate the effect of thermal treatment of EN on the contact angles, the deposited EN were annealed at 350°C for 1 to 3 h. With respect to the oxidation of Ni, the Gibbs free energy for formation of NiO at 350°C can be evaluated.

$$\begin{aligned} Ni + O_2 &\rightarrow NiO \\ \Delta G^0_{f,600K} &\rightarrow 184 \text{ KJ/mole} \\ \Delta G^0_{f,700K} &\rightarrow -175 \text{ KJ/mole} \end{aligned} \quad (4)$$

By interpolation, the energy of reaction at 350°C is then

$$\Delta G_{r,623K} = \Delta G^0_{f,623K} + RT \ln\left[\frac{a_{NiO}}{a_{Ni} P^{1/2}_{O_2}}\right] \quad (5)$$

where $\Delta G_{f,\,623K}$ is Gibbs free energy for formation of NiO at 623 K; $\Delta G_{r,\,623\,K}$ is Gibbs free energy for reaction of NiO at 623 K; a_{Ni} is the activity of Ni, assumed to be unity; a_{NiO} is the activity of NiO, assumed to be unity; P_{O_2} the partial pressure of oxygen in the atmosphere, approximated by O_2 atm.

Thus, $\Delta G_{r,\,623\,K}$ is calculated to be –179 KJ/mole. Oxidation of Ni occurs spontaneously at 350°C.

For the EN surfaces without RMA cleaning, the presence of NiO is evident for oxygen is found through Auger analysis. Since the oxygen content is less than 10% by Auger analysis, ESCA x-ray photo spectroscopy (XPS) was further used for better sensitivity. The results show an increase in oxygen contents from –10 at.% to –30 at.% in the Sn-Bi/EN(8.52 wt.% P – 13.3 wt.% P) joint annealed at 350°C for 1 to 3 h, respectively.

Contact angles of lead-free solders on the annealed EN approach 180° if RMA flux is not used when soldering to EN. The formation of NiO develops a poor adhesion between the solder and the Ni-P/Al_2O_3 substrate. Thus, the solder drops appear almost non-wetting on the Ni-P/Al_2O_3 substrates.

The x-ray diffraction (XRD) patterns of Ni-P/Al_2O_3 substrates annealed in air at 350°C for various times are shown in Figs. 15 and 16, for deposition pH value at 4.0 and 6.0, respectively. Peaks of Ni-P precipitation appear and the intensity of Ni_3P peak on the EN surface is enhanced upon longer annealing times and lower phosphorus content. On the basis of the binary Ni-P phase diagram,[18] Ni_3P, the major precipitated phase during heat treatment at 350°C, is a stable phase.

In order to investigate the effect of precipitate Ni_3P on wetting behavior, RMA flux was used to remove the NiO layer. Figure 17 shows the variation of contact

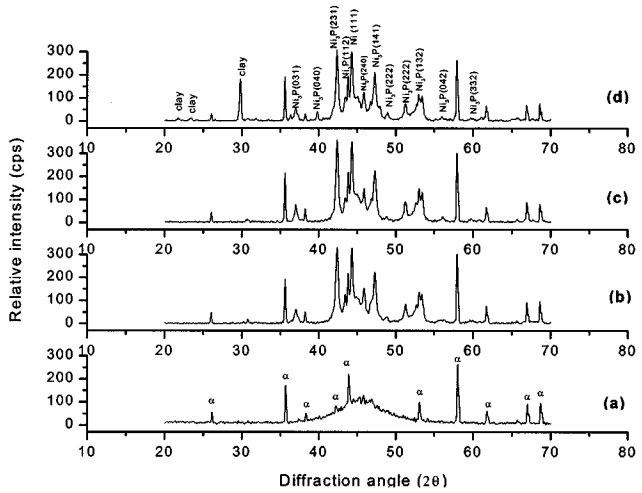

Fig. 15. The XRD patterns for EN plated with a pH value of 4.0 annealed at 350°C for various time, (a) as-deposited, (b) 1 h, (c) 2 h, and (d) 3 h.

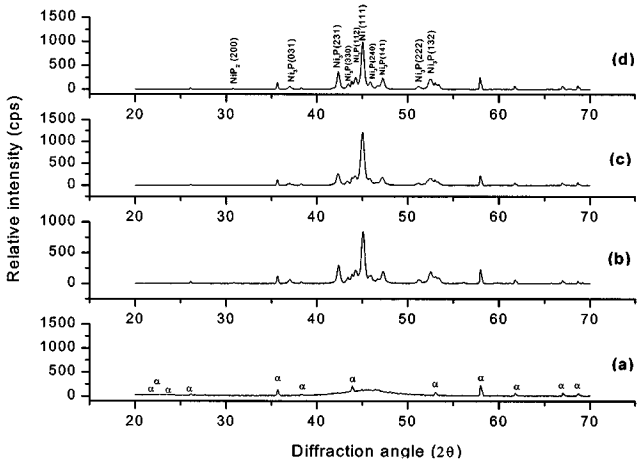

Fig. 16. The XRD patterns for EN plated with a pH value of 6.0 annealed at 350°C for various time, (a) as-deposited, (b) 1 h, (c) 2 h, and (d) 3 h.

angles of lead-free solders in the Ni-13.3 wt.%P/Al_2O_3 joint with different degrees of Ni_3P precipitates. For the Sn/EN (13.3 wt.%P) joint annealed at 350°C, the amount of Ni_3P precipitates in EN increase with the annealing time as evidenced from the XRD peaks in Fig. 15. Figure 17a indicates that the contact angle between Sn and EN (13.3 wt.%P) increases in proportion to the annealing time, and the effect of Ni_3P on the contact angle is evident. For Sn-Ag/EN (13.3 wt.%P) and Sn-Bi/EN (13.3 wt.%P) joints after EN annealing, non-wetting occurs with the contact angle greater than 100° as indicated in Fig. 17b and c. Table V lists the measured contact angles in the solder/EN (8.52 wt.%P) joint, non-wetting also occurs as long as EN is annealed. Figure 18a and b show the schematic diagram for surface tension equilibrium between the solder and EN metallized substrates with the presence of NiO and Ni_3P, respectively. According to the Young-Durpe equation, Fig. 18a reveals

$$\gamma_{sf} - \gamma_{1\text{–}NiO} = \gamma_{lf} \cos\theta_1 \quad (6)$$

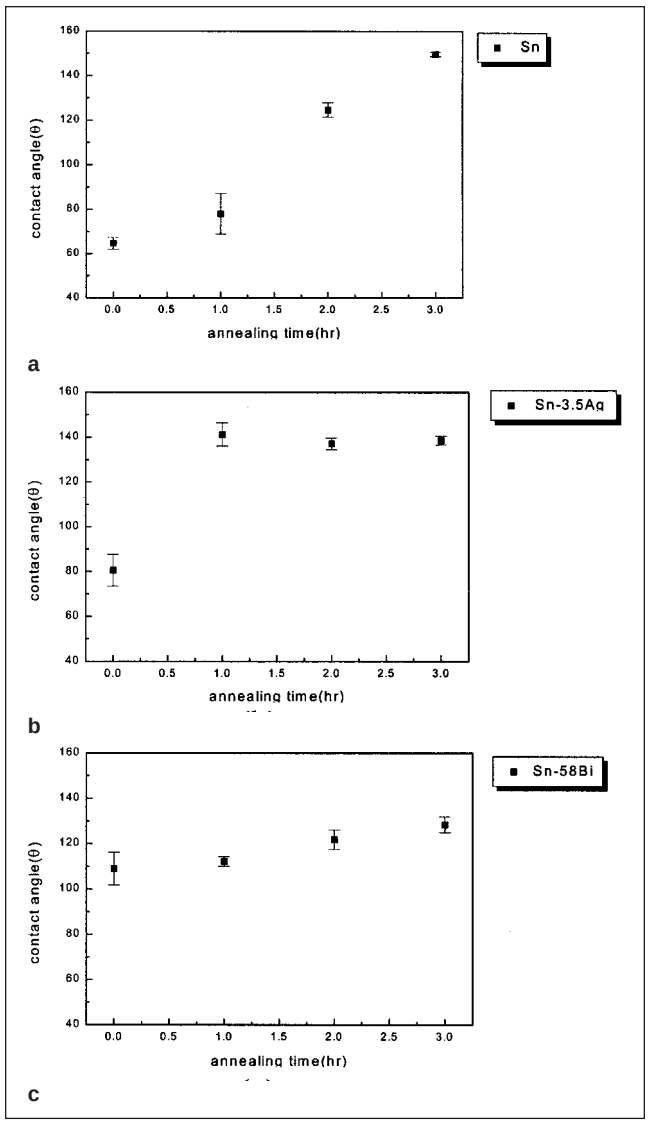

Fig. 17. Contact angles of lead-free solders, (a) pure Sn, (b) Sn-3.5Ag, and (c) 42Sn-58Bi, on EN(13.3wt.%P)/Al_2O_3 substrates annealed at 350°C.

where θ_1 is the equilibrium contact angle, γ_{sf} is the surface tension between solid substrate and flux, $\gamma_{1\text{–}NiO}$ is the surface tension between liquid solder and NiO; and γ_{lf} is the surface tension between liquid solder and flux. Similarly in Fig. 18b

$$\gamma_{sf} - \gamma_{1\text{–}Ni_3P} = \gamma_{lf} \cos\theta_2 \quad (7)$$

where θ_2 is the equilibrium contact angle, γ_{sf} is the surface tension between solid substrate and flux, $\gamma_{1\text{–}Ni_3P}$ is the surface tension between liquid solder and Ni_3P, and γ_{1f} is the surface tension between liquid solder and flux. After rearrangement of Eqs. 6 and 7

$$\gamma_{lf} \cos\theta_1 + \gamma_{1\text{–}NiO} = \gamma_{lf} \cos\theta_2 + \gamma_{Ni_3P} \quad (8)$$

Experimentally, it was found that $\theta_1 > \theta_2$. Thus, it is argued that $\gamma_{1\text{–}NiO} > \gamma_{1\text{–}Ni_3P}$, since γ_{1f} remains the same in both cases.

Table V. The Contact Angle of Lead-Free Solders on EN (8.52 wt.%P)/Al_2O_3 Substrates After Annealing at 350°C

Alloy	Annealing Time (hr)			
Sn	78.3± 4.2	147.9 ± 3.5	142.7 ± 0.2	141.1 ± 2.2
Sn-3.5Ag	82.3 ± 2.5	139.5 ± 1.2	139.6 ± 2.1	135.4 ± 0.7
42Sn-58Bi	121.7 ± 0.9	120.7 ± 1.8	126.2 ± 2.0	126.5 ± 1.9

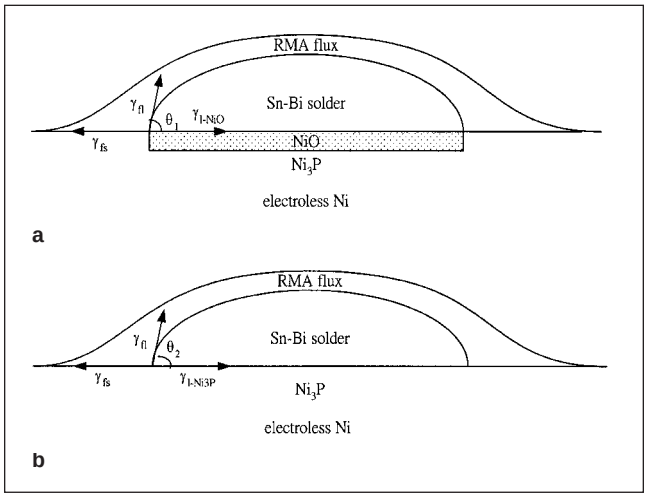

Fig. 18. Schematic diagram for the surface tension equilibrium between the solder and EN metallized substrate, with the presence of (a)NiO and (b) Ni_3P.

In summary, the wettability of several unleaded solders on oxidized EN is substantially degraded due to the presence of NiO. Similarly, non-wetting also takes place in the presence of Ni_3P if EN is annealed at 350°C for several hours. Consequently, to use Pb-free solders on the electroless Ni, oxidation and precipitation of EN should be prevented to achieve a better wetting behavior.

CONCLUSIONS

The contact angles of pure Sn solder on the electroless Ni (EN) with 6.0–12.0 wt.%P ranged from 45° to 70°. For Sn-3.5Ag/EN and 42Sn-58Bi/EN joints, the contact angles were 60–90° and 80–125°, respectively. For all three lead-free solders, wettability was degraded as the phosphorous contents in EN were reduced. The variation of contact angles in the solder/EN joint with respect to the phosphorous contents in EN might be due to the surface morphology and density of EN with various pH values during deposition, as well as the interfacial reaction between the solders and EN. A region of solid solution Sn-Bi-Ni-P was observed near the interface of solder/EN. The concentration profile evaluated by EPMA revealed the interdiffusion of Sn and Ni. There also existed an enrichment of P near the solder/EN interface. Wettability of Sn-Bi/EN (9.2 wt.%P) joints was improved as the soldering temperature increased. The contact angle could be reduced to around 40–50° if the soldering temperature was raised above 200°C. Wettability in Sn/EN, Sn-Ag/EN and Sn-Bi/EN joints with Ni_3P precipitate after annealing at 350°C for several hours was better than that with the presence of NiO due to oxidation. Nevertheless, contact angles in solder/EN joints with Ni_3P precipitate were larger than those in solder/as-deposited EN joints.

ACKNOWLEDGEMENT

The financial support from National Science Council under the contract No. NSC-89-2216-EO07-041 is acknowledged.

REFERENCES

1. R.C. Marrs, B. Freyman, and J. Martin, *Electron. Manuf. Technol. Symp.* (Piscataway, NJ: IEEE, 1993), p. 41.
2. Z. Mei, M. Kaufmann, A. Eslambolchi, and P. Johnson, *Proc. 48th Electron. Components and Technol. Conf.* (Piscataway, NJ: IEEE, 1998), p. 952.
3. R.C. Marrs, *Proc. 2nd Int. Conf. and Exhibition on Multichip Modules* (Piscataway, NJ: IEEE, 1993), p. 220.
4. R.C. Groover, C. Huang, and A. Hamzehdoost, *Proc. 1st Int. Symp. Flip Chip Technol.*, 1994, p. 57.
5. D.R. Frear, F.M. Hosking, and P.T. Vianco, *Materials Developments in Microelectronic Packaging and Reliability* (Materials Park, OH: ASM, 1991, 1991), p. 229.
6. C.Y. Lee and K.L. Lin, *Thin Solid Films* 249, 201 (1994).
7. C.Y. Lee and K.L. Lin, *Jpn. J Appl. Phys.* 33, 4708 (1994).
8. D.W. Baudrand, *Plating and Surface Finishing* 68, 57 (1981).
9. J. Glazer, *Int. Mater. Rev.* 40, 65 (1995).
10. S.K. Kang, R.S. Rai, and S. Purushothaman, *J. Electron. Mater.* 25, 1113 (1996).
11. T. Massalski, *Binary Alloy Phase Diagram* (Materials Park, OH: ASM, 1986), p. 540.
12. K.L. Lin and J.M. Jang, *Mater. Chem. and Phys.* 38, 33 (1994).
13. H.W. Miao, M.S. Thesis, National Tsing Hua University, Hsinchu, Taiwan (1997).
14. Y.Y. Wei, M.S. Thesis, National Tsing Hua University, Hsinchu, Taiwan (1997).
15. J.H. Vincent, B.P. Richards, D.R. Wallis, I.A. Gunter, M. Wasewick, H.A. Steen, P.G. Harris, M.A. Whitmore, S.R. Billington, A.C. Harman, and E. Knight, *Circuit World* 19, 32 (1997).
16. C.D. Young, Ph.D. Dissertation, National Tsing Hua University, Hsinchu, Taiwan (1997).
17. R.B. Bird, W.E. Stewart, and E.N. Lightfoot, *Transport Phenomena* (New York: John Wiley & Sons, 1960), p. 29.
18. P. Nash, P*hase Diagram of Binary Nickel Alloy* (Materials Park, OH: ASM, 1991), p. 235.
19. R.N. Wenzel, *Ind. Eng. Chem.* 28, 988 (1936).
20. R. Shuttleworth and G.L.J. Bailey, *Disc. Faraday Soc.* 3, 16 (1948).
21. R.H. Dettre and R.E. Johnson, *Ave. Chem. Ser.* 43, 112 (1963).
22. C. Huh and S.G. Mason, *J. Colloid Interface Sci.* 60, 11 (1977).
23. J.D. Eik and R.J. Good, *J. Colloid Interface Sci.* 53, 235 (1975).
24. X.B. Zhou and J.Th. M. DeHosson, *J. Mater. Res.* 10, 1984 (1995).
25. Y.Y. Chen, J.G. Duh, and B.S. Chiou, *J. Mater. Sci.: Mater. Electron.* 11, 279 (2000).